FIRE AND MATERIALS
Fire Mater. 2016
Published online in Wiley Online Library (wileyonlinelibrary.com). DOI: 10.1002/fam.2390

Analytical and numerical assessments of local overpressure from hydrogen gas explosions in petrochemical plants

Boohyoung Bang[1,2], Hyunsu Park[2], Jonghun Kim[3], Salem S. Al-Deyab[4], Alexander L. Yarin[1,5,*,†] and Sam S. Yoon[1,*,†]

[1]*School of Mechanical Engineering, Korea University, Seoul 136-713, Korea*
[2]*Plant and Environmental Research Team, Daewoo Institute of Construction Technology, Suwon, Kyungki-do 440-210, Korea*
[3]*Process Engineering Team, Daewoo Engineering and Construction, Seoul 110-713, Korea*
[4]*Petrochemical Research Chair, Department of Chemistry, College of Science, King Saud University, Riyadh 11451, Saudi Arabia*
[5]*Department of Mechanical and Industrial Engineering, University of Illinois at Chicago, 842 W. Taylor St., Chicago 60607, IL, USA*

SUMMARY

Accurate prediction of pressure rise is important for safety assessments of a petrochemical plant in the event of an explosion accident. The sudden pressures arising from gas explosions at various hydrogen concentrations in air have been predicted analytically and numerically. These solutions were compared against experimental data. The analytical solution, based on the self-similar solution for pointwise strong explosions in an open space, which assumed no energy loss and premixed fuel-air mixture, reasonably predicted the explosive-ignition detonation case while the numerical solutions were more suitable to model spark-ignition deflagration cases that accounted for the effect of turbulence arising from three-dimensionality and presence of obstacles in the computational domain. Comparison of both analytical and numerical results against experimental data indicates that their differences are within a 30% margin. The analytical model presented herein can be useful for field engineers who want conservative estimates of the overpressure resulting from explosive-ignition detonation. Copyright © 2016 John Wiley & Sons, Ltd.

Received 10 January 2016; Revised 9 May 2016; Accepted 17 July 2016

KEY WORDS: petrochemical plant; gas explosion; overpressure; analytical solution

1. INTRODUCTION

In petrochemical plants, unexpected releases of combustible vapors/gases can lead to explosions, which threaten the integrity of equipment and structures. Multiple explosions can destroy plants, jeopardize lives, and inflict large economic losses; outdated parts of the pipe system can leak flammable gas in air and pose the danger of explosion as illustrated in Figure 1 [1, 2]. Therefore, it is important to be able to predict explosion properties and to design pipes and storage tanks that can withstand such catastrophic events. Such efforts enable plant engineers to evaluate risks associated with their designs subject to various possible explosions. Pressure rises almost instantaneously because of the overpressure from an explosion causing structural damage or deformation of pipes and storage tanks. Explosive pressure and structural damage can be estimated with analytical and numerical tools. By using these computational tools, safe distances between equipment and structures can be assigned.

*Correspondence to: Alexander L. Yarin and Sam S. Yoon, School of Mechanical Engineering, Korea University, Seoul 136-713, Korea.
†E-mail: skyoon@korea.ac.kr; ayarin@uic.edu

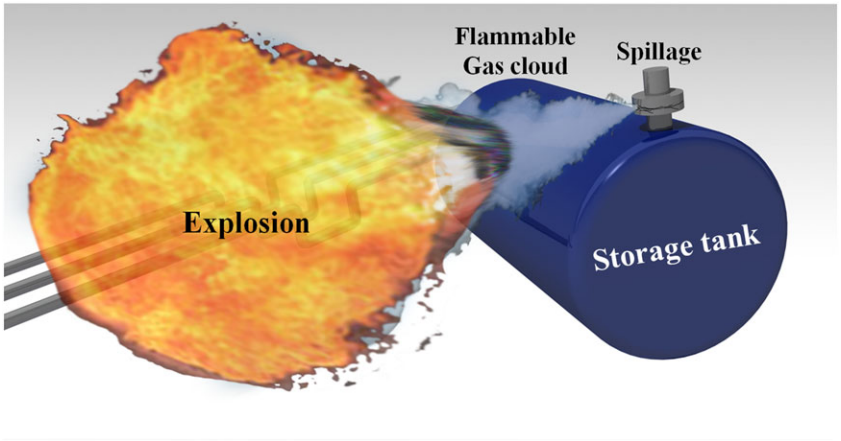

Figure 1. Schematic of an explosion and its effects.

It is easy to envision how a flammable vapor could leak into an unconfined/open area of a plant. If the leaked fuel concentration in air is low and the vapor cloud is diluted, explosion is unlikely to occur, especially if unobstructed and far from nearby structures. However, one must consider the worst-case accident scenario; case in point is a large mass of a flammable gas in the scale up to a few hundred kg well mixed in air in stoichiometric ratio in a confined space. This amount of leakage of the flammable gas may arise when safety alert systems fail during an unexpected circumstance such as a terrorist attack. In this worst-case scenario, flame velocity is high, and deflagration almost immediately changes to detonation, resulting almost instantaneously in a powerful explosion and formation of a shock wave propagating in air. The evaluation of the worst-case accident scenario should be accounted for when structural designs are developed. This is needed for a conservative estimate of the safety-related issues associated with design of equipment and structures so that they can withstand such a harsh explosive environment.

Explosive pressure can depend on several factors, such as fuel type, fuel mass, the fuel–air ratio, location of the ignition point, the ignition-source strength, the presence of surrounding obstructions, shock wave propagation, turbulence developing in air, and ambient winds. Most aspects can be taken into account using a computational fluid dynamics code, such as FLame ACceleration Simulator (FLACS), which simulates a release of gas and its subsequent explosion. FLACS has been preferred by plant engineers for its long history of reliable use in both onshore and offshore applications.

Molkov *et al*. [3] developed Large Eddy Simulation code to model the hydrogen–air deflagration in a 20-m diameter unconfined hemispherical shell. They commented that sufficient grid resolution with adaptive regriding would be more accurate, although their results seemed satisfactory when they were compared with their experimental data. Middha and Hansen [4] overviewed the recent validation studies for FLACS in hydrogen explosion cases in response to the stringent hydrogen safety code and quantitative risk assessment challenges. They noted that FLACS produces reasonable predictions for various kinds of geometries and conditions. Davis *et al*. [5] also noted that FLACS was helpful to understand the chain-reaction-driven explosion and the near-field blast damage. These findings eventually led to identifying the explosion origin in the manufacturing factory in Danvers, Massachusetts, in 2006. Garcia *et al*. [6] compared various 3D computational tools to model the explosion of a hydrogen–air mixture in a balloon of 10-m radius.

Although FLACS is a powerful computational tool that simulates gaseous explosions, it cannot simulate detonation phenomena, in particular, the explosive ignition (or strong explosion) case, for which the analytic self-similar solution should be used. The classical theory of strong explosions implies an instantaneous, pointwise release of the explosion energy and thus allows for an analytical solution for the gas dynamics of the resulting gas flow [7–13]. In particular, it predicts the pressure, gas velocity, and density at the shock wave front. For this reason, the capability of FLACS and the

DOI: 10.1002/fam

analytic self-similar solution in predicting the overpressure for deflagration and detonation cases, respectively, has been evaluated in this work.

The experimental data on hydrogen concentration and ignition type of hydrogen–air mixtures in an open space will be used for comparison. A quiescent, homogenous mixtures of 20% to 30% hydrogen by volume filling 5.2 and 37-m^3 tents were employed in the experiments of [14]. In these experiments, a stoichiometric (30%) and lean (20%) hydrogen–air mixtures were ignited by a spark, which produced deflagration. When ignited by an explosive, the flame was categorized as 'detonation'. Further details on the experiment are available in Section 3.1. In Section 3.2, the FLACS prediction of the overpressure at varying hydrogen mass has been presented.

2. MODELING DESCRIPTION

2.1. Numerical simulation of weak explosions by FLACS

In general, the pressure rise and the resulting overpressure are expected to be estimated from both computational and experimental studies because these parameters determine structural damage. For a fuel vapor cloud explosion at a petrochemical plant, which occupies a significant space and thus is dilute, devastating supersonic detonation is not anticipated, and in such unconfined/open area, cloud overpressures do not exceed a few bar. This relatively weak explosion case is considered deflagration. The flame front, as is well known, generates turbulence, as well as the surrounding obstacles generate turbulence, thereby increasing the burning rate. This, in turn, results in fast deflagration wave/flame propagation further increasing turbulence.

2.1.1. Governing equations. The governing equations used in FLACS include the mass (1), momentum (2), enthalpy balances (3), the fuel balance (4), the turbulent kinetic energy balance (5), and Eq. (6) for dissipation rate of turbulent kinetic energy as introduced in [15]. The size of the computational domain was $200 \times 200 \times 100\,m^3$, which replicated the actual plant including a gas central processing unit and other additional facilities. A total number of the 2-million computational nodes were used. The Courant-Friedrich-Levy (CFL) number of 0.5 was used to secure numerical stability. The simulation duration was limited to 1 s.

$$\frac{\partial}{\partial t}(\beta_v \rho) + \frac{\partial}{\partial x_j}\left(\beta_j \rho u_j\right) = \frac{\dot{m}}{V} \tag{1}$$

$$\frac{\partial}{\partial t}(\beta_v \rho u_i) + \frac{\partial}{\partial x_j}\left(\beta_j \rho u_i u_j\right) = -\beta_v \frac{\partial P}{\partial x_i} + \frac{\partial}{\partial x_j}\left(\beta_j \sigma_{ij}\right) + F_{o,i} + \beta_v F_{w,i} + \beta_v(\rho - \rho_0) g_i \tag{2}$$

$$\frac{\partial}{\partial t}(\beta_v \rho h) + \frac{\partial}{\partial x_j}\left(\beta_j \rho h u_j\right) = \frac{\partial}{\partial x_j}\left[\beta_j \frac{\mu_{eff}}{\sigma_h}\frac{\partial h}{\partial x_j}\right] + \beta_v \frac{DP}{Dt} + \frac{\dot{Q}}{V} \tag{3}$$

$$\frac{\partial}{\partial t}\left(\beta_v \rho \Upsilon_{fuel}\right) + \frac{\partial}{\partial x_j}\left(\beta_j \rho u_j \Upsilon_{fuel}\right) = \frac{\partial}{\partial x_j}\left[\beta_j \frac{\mu_{eff}}{\sigma_{fuel}}\frac{\partial \Upsilon_{fuel}}{\partial x_j}\right] + R_{fuel} \tag{4}$$

$$\frac{\partial}{\partial t}(\beta_v \rho k) + \frac{\partial}{\partial x_j}\left(\beta_j \rho u_j k\right) = \frac{\partial}{\partial x_j}\left[\beta_j \frac{\mu_{eff}}{\sigma_k}\frac{\partial k}{\partial x_j}\right] + \beta_v P_k - \beta_v \rho \varepsilon \tag{5}$$

$$\frac{\partial}{\partial t}(\beta_v \rho \varepsilon) + \frac{\partial}{\partial x_j}\left(\beta_j \rho u_j \varepsilon\right) = \frac{\partial}{\partial x_j}\left[\beta_j \frac{\mu_{eff}}{\sigma_\varepsilon}\frac{\partial \varepsilon}{\partial x_j}\right] + \beta_v P_\varepsilon - C_{2\varepsilon}\beta_v \rho \frac{\varepsilon^2}{k}, \tag{6}$$

where $F_{o,i}$ is flow resistance because of sub-grid obstructions and $F_{w,i}$ is flow resistance because of walls. Also, β_v is volume porosity, β_j is area porosity, ρ is the density of the gas mixture, x_i are the Cartesian coordinates, u_i are the velocity components, $\dot{m}$ is mass release rate, V is volume where the

DOI: 10.1002/fam

mass is released, g is gravity acceleration, P is pressure, and σ_{ij} is the stress tensor. In addition, $\dot{Q}$ is the rate of heat release in the combustion reaction and R_{fuel} is the fuel reaction rate.

Constants required for the k-ε turbulence model are taken from [16]. The compressible 3D Navier–Stokes equations are solved by using a finite-volume method in FLACS. References [17, 18] describe the implementaton of the basic equations, and [19] presents the experimental data on explosion used to validate FLACS. FLACS uses a second order scheme for resolving diffusive terms and a second order hybrid scheme to resolve convective terms. The time marching steps are advanced by a first order backward Euler scheme to secure numerical stability. The Semi-Implicit Method for Pressure-Linked Equations (SIMPLE) pressure-correction algorithm [20] is applied and modified to extend its scheme to compressible flows with extra source terms, which accounts for the work term by compression in the enthalpy equation. Iterations are applied until residuals are less than a certain tolerance.

When a combustible cloud is ignited close to the quiescent conditions, the initial burning process is laminar. The flame front is smooth, and the flame propagation is entirely governed by thermal and/or molecular diffusion processes [21]. Shortly after this stage, instabilities originating from various sources (e.g., ignition, flow dynamics, and the Rayleigh–Taylor instability) warp the flame surface resulting in an increased, quasi-laminar flame speed. Depending on the flow conditions, the deflagration front can accelerate and create a shock wave, which is sustained by the exothermic chemical reaction behind its front; that is, deflagration wave can transform itself into a detonation wave. Such a transition can happen in the turbulent burning regime. The laminar burning velocity depends on the type of fuel, fuel–air mixture, and pressure. The laminar burning velocities at different equivalence ratios are tabulated for various fuels, and the laminar burning velocity of a fuel mixture is calculated as the volume-weighted average. In the quasi-laminar regime, the turbulent burning velocity is computed. Then the turbulent burning velocity is a simplified form of the expression available in [22], where the Karlovitz stretch factor including the turbulent Reynolds number is used.

2.1.2. Combustion models. Ignition is initiated when flammable gas concentration is sufficiently high. Once ignited, laminar burning velocity is calculated, associated with chemical reactions of combustion. The turbuence model (turbulent burning velocity) is triggered by the Rayleigh–Taylor instability at the flame–air interface and associated with the flow field and wall shear stresses, buoyancy, sub-grid object models, etc.

Ignition of a premixed cloud of fuel and oxidant may escalate to an explosion, but before that, the laminar burning velocity is as follows:

$$S_L^0 = S_L^0(\text{fuel}, \Phi), \tag{7}$$

which depends on the fuel and the equivalence ratio. For mixtures with fuel contents outside of the lower and upper flammability limits, the laminar burning velocity is zero (they will not burn). In an explosion, the flame accelerates and becomes turbulent with a significantly higher burning velocity because of the improved mixing of reactants and products. FLACS uses correlations for both laminar and turbulent burning velocities derived from experimental work.

Because the reaction zone in a premixed flame is thin compared with the grid resolution, the flame zone is thickened by increasing the diffusion and reducing the reaction rate by factors of β (the β-model).

2.1.3. Flame model. The diffusion coefficient in the transport equation for fuel is as follows:

$$D = \frac{\mu_{eff}}{\sigma_{fuel}}. \tag{8}$$

In the β-model, the dimensionless reaction rate, W, and diffusion coefficient are adjusted as follows:

$$W^* = \frac{W}{\beta} = W\frac{l_{LT}}{\Delta_g}, \tag{9}$$

$$D^* = D\beta = D\frac{\Delta_g}{l_{LT}}. \tag{10}$$

DOI: 10.1002/fam

From an eigenvalue analysis of the burning velocity [23], the relation between D and W is as follows:

$$WD = 1.37S_u^2 W^* D^*, \tag{11}$$

where $\chi_q = 0.05$ is the quenching limit of the progress variable χ. D^* and W^* depend on grid size and the burning velocity as as follows:

$$W^* = c_{1\beta}\frac{S_u}{\Delta_g}, \tag{12}$$

$$D^* = c_{2\beta}S_u\Delta_g. \tag{13}$$

The reaction rate of fuel is estimated as follows:

$$R_{fuel} = -W^*\rho\min\left[\delta_H\left(\chi - \chi_q\right), \chi, 9 - 9\chi\right], \tag{14}$$

where δ_H is the Heaviside step function.

2.1.4. Burning velocity model. Laminar burning velocity is a function of pressure:

$$S_L = S_L^0\left(\frac{P}{P_0}\right)^{\gamma_P}, \tag{15}$$

where γ_P is a fuel-dependent parameter. In the quasi-laminar regime, the turbulent burning velocity is as follows:

$$S_{QL} = S_L\left\{1 + a\min\left[\left(\frac{R}{3}\right)^{0.5}, 1\right]\right\}, \tag{16}$$

where R is the flame radius and a is a fuel-dependent constant.

The turbulent burning velocity is a simplification of the general expression presented by [22],

$$\frac{S_T}{S_L} = 0.875K^{-0.392}\frac{u'}{S_L}, \tag{17}$$

where K is the Karlovitz stretch factor including the turbulent Reynolds number. FLACS selects burning velocity as follows:

$$S_u = \max\left(S_{QL}, S_T\right). \tag{18}$$

2.2. Analytical simulation of strong explosions

After the escape of a flammable gas, it mixes with the surrounding air yielding a premixed flame explosion scenario. Once the fuel–air cloud explodes/ignites instantaneously on a large scale, a shock wave propagates in the surrounding gas. Pressure and temperature behind the shock wave front are high, and if the chemical reaction at its front could continue, it can create a self-sustaining detonation wave. A sonic or supersonic detonation wave is sustained by the combustion reactions at the shock wave front and propagates into an unburned gas at speeds of 1500 to 2000 m/s resulting in overpressures in the 15 to 20-bar range. The classical theory of strong explosions, however, implies that the chemical reaction is over instantaneously (at the moment of strong explosion) and deals with propagation of the shock wave alone. The theory of strong explosions specifies, among other parameters, the pressure, P_{sh}, gas velocity, V_{sh}, and density, ρ_{sh}, at the shock wave front as [7–13]:

$$P_{sh} = \frac{8\rho_a}{25(\gamma+1)}\left(\frac{E_0}{\rho_a}\right)^{2/5}\frac{1}{t^{6/5}}, \tag{19}$$

$$V_{sh} = \frac{4}{5(\gamma+1)}\left(\frac{E_0}{\rho_a}\right)^{1/5}\frac{1}{t^{3/5}}, \tag{20}$$

and

DOI: 10.1002/fam

$$\rho_{sh} = \frac{(\gamma+1)}{(\gamma-1)}\rho_a. \tag{21}$$

where E_0 denotes the total energy released in the explosion, ρ_a is the air density before the shock wave, γ is the ratio of the specific heat at constant pressure to the specific heat at constant volume (of air), and t is time from the moment of explosion, which is considered to happen instantaneously and pointwise at $t=0$. These analytic solutions are applicable for perfectly spherical strong explosions alone.

Accordingly, the front of the shock wave, which is spherical when unaffected by obstacles, r_{sh}, is as follows:

$$r_{sh} = \frac{2}{(\gamma+1)}\left(\frac{E_0}{\rho_a}\right)^{1/5} t^{2/5}. \tag{22}$$

The strong-explosion theory is based on the assumption that the explosion energy, E_0, is released instantaneously at a point. This implies that fuel is instantaneously evaporated and mixed with the oxidizer, and the reacting mixture is stoichiometric. The theory also neglects energy losses due to thermal radiation – all energy is preserved. These assumptions tend to overestimate the strength of the shock wave. In reality, liquid methane spillage and evaporation, for example, will take some time and space and are accompanied by liquid atomization (losses). Also, mixing with the oxidizer (oxygen in air) can be far from complete when the explosion occurs, and nitrogen in air will act as a thermal ballast. Typically, a fuel–oxidizer mixture will not be fully premixed. These factors diminish the strength of a real shock wave compared with these ideal predictions. The strong-explosion theory is purely gas dynamical and does not consider turbulent eddy viscosity and the effect of turbulence on the energy-release rate. As it stated before, the strong-explosion theory does not imply formation of a self-sustaining detonation wave because the chemical reaction is assumed to be over instantaneously. With all the simplifying assumptions listed previously, the first estimates of the strong explosion effects should be based on the strong-explosion theory outlined above.

Based on Eqs. (19) and (20), the time required for the shock wave to reach a pipe located a distance L from the center of explosion is as follows:

$$t = L^{5/2}\left(\frac{\gamma+1}{2}\right)^{5/2}\frac{1}{(E_0/\rho_a)^{1/2}}. \tag{23}$$

The pressure and velocity of the shock-wave front as it contacts the pipe are as follows:

$$P_{sh,L} = \frac{64}{25}\ \frac{1}{(\gamma+1)^4}\ \frac{E_0}{L^3}, \tag{24}$$

and

$$V_{sh} = \frac{4\sqrt{8}}{5}\frac{1}{(\gamma+1)^{5/2}}\frac{1}{L^{3/2}}\left(\frac{E_0}{\rho_a}\right)^{1/2}. \tag{25}$$

A recent example of prediction of the effect of a shock wave generated by a strong explosion on pipelines in petrochemical plants can be found in Bang *et al*. [24].

3. RESULTS AND DISCUSSION

3.1. Comparison with experiments

Table I summarizes the case studies we have conducted herein. Because Cases A and B are deflagrations, these experimental data are compared with FLACS simulations. Because the analytical solution was obtained for an almost instantaneous explosion reminiscent of detonation, it is compared with Case C. Cases 1 and 2 reflect small and large volumes corresponding to 5.2 and 37 m^3 of the hydrogen/air mixture in a confined plastic tent, respectively.

DOI: 10.1002/fam

Table I. Case studies compared with experimental results.

Calculation	FLACS Spark (deflagration)		Equation (24) Explosive (detonation)
Ignition type Hydrogen concentration (mixture type)	A (lean)(%)	B (stoichiometric)	C (stoichiometric) (%)
Case 1 ($5.2\,m^3$)	20	30	30
Case 2 ($37\,m^3$)	20	30	30

FLACS, FLame ACceleration Simulator.

In the experiment, overpressure was recorded using PCB Piezotronics model 133A36, 137A23, and 112 M343 quartz pressure transducers (PCB Piezotronics, Inc., Walden Avenue, Depew, NY, USA), which were installed at increasing distances from the ignition source. Pressure measurements at R reflect blast wave travel times. The blast wave travels subsonically and supersonically for deflagration or detonation, respectively. Both deflagration (Cases A and B) and detonation (Case C) ignitions are considered; Cases A and B were ignited by a spark, and Case C was ignited by an explosive. The spark was generated with a 40-J capacitive discharge unit while a 10-g booster of C-4 explosive (5.2×10^4 J) was used to detonate the stoichiometric mixture with 30% hydrogen volume. Masses of 20% hydrogen by volume are considered 'lean' while 30% hydrogen by volume is considered 'stoichiometric' when mixed with air. The mixtures are assumed homogenous and quiescent.

Figure 2a compares the numerical results from FLACS to the experimental data of [14] for Case A, which is a lean deflagration case. The x-axis indicates the distance away from the ignition point, normalized by the characteristic length defined as $R_0=(E_0/P_0)^{1/3}$, where E_0 is the combustion energy (LHV, Lower Heating Value) of hydrogen, and P_0 is atmospheric pressure. This parameter is known as the Sachs-scaling distance, which is a common standard [25]. Their curvatures and overpressure appear to be consistent, but their absolute overpressure values moderately differ, except the starting and end points. The FLACS simulation appears to underpredict the experimental results in case of the lean combustion case. However, as for the stoichiometric case B, their difference is greatly reduced; see Figure 2b. The FLACS simulation still underpredicts the experimental data; however, the prediction is much closer to the experimental data, as compared with the lean combustion case A.

FLame ACceleration Simulator does not account for the subtle difference in the ignition energy. FLACS simply assumes ignition is initiated when flammable gas concentration is higher than a certain threshold, which is in general set by a software user. FLACS assumes ignition of a premixed cloud of fuel and oxidant. When this concentration of premixed cloud is low (such as Cases A), the degree of the explosion of this lean combustion case in FLACS cannot be up to the level of the real (or experimental) combustion, which is the shortcoming of FLACS. However, when the concentration of the premixed cloud is high (such as Case B), the comparison between FLACS predictions and experimental data has improved significantly; see Figure 2b. This excellent agreement indicates FLACS accurately predicts the overpressures resulting from deflagration when the fuel–air concentration is relatively high. In addition, it should be emphasized that FLACS semi-empirically accounted for the effect of the generated turbulent eddies on the flame propagation, as well as the detailed kinetics of the combustion reaction, which in turn helps the model to realistically match the experimental data.

In Figure 2c, the detonation case C has been studied by comparing the analytic predictions for a shock wave produced by a strong explosion against the experimental data. The comparison shows good agreement. There are two reasons for that. First, the analytic self-similar solution corresponds to a pointwise strong explosion in an open spherical space, which is very close to the experimental case C. Second, it stems from the fact that the chemical reaction behind the shock wave front rapidly expires, and a pure shock wave rather than a detonation wave arises, even though the real explosion was not exactly instantaneous.

As shown in Figure 2a,b, the experimental overpressure data are relatively insensitive to the total volume of hydrogen as there are no discernable difference between Cases 1 and 2 regardless of whether the ignition was by spark or detonation. However, FLACS simulations indicate differences between Cases 1 and 2. Overpressure from the large volume ($37\,m^3$, solid curves) is greater than

DOI: 10.1002/fam

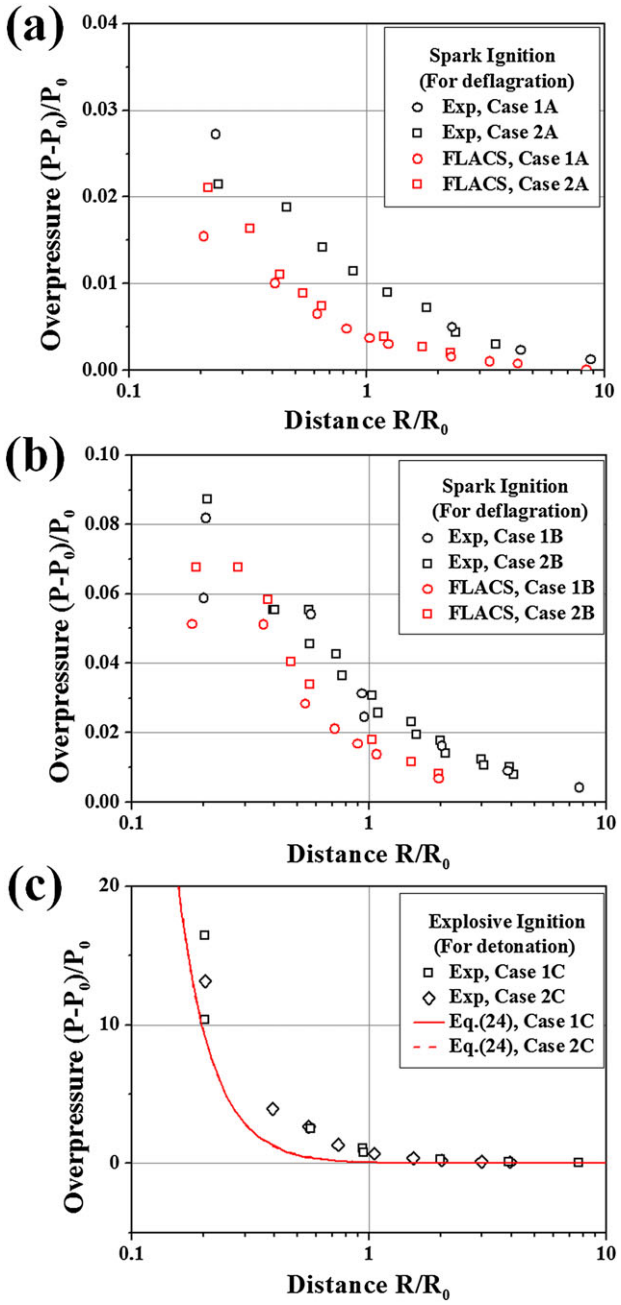

Figure 2. Simulated overpressures compared with experimental data. (a) Case A: spark ignition (deflagration) lean mixture type, (b) Case B: spark ignition (deflagration) stoichiometric mixture type, (c) Case C: explosive ignition (detonation) stoichiometric mixture type.

overpressures from the small volume (5.2 m^3, dashed curves) because more hydrogen yields a more powerful blast wave.

Figure 3 quantifies the deviation of the simulations from the data at $R/R_0 \leq 0.4$, which appears to be satisfactory, considering the uncertainties associated with both numerical predictions and experimental data.

3.2. Uncertainty comparison

To estimate the potential damage from an unexpected explosion, the explosive pressure increase and consequent deformation of surrounding pipes and tanks are assessed. Figure 4 is pressure

DOI: 10.1002/fam

distributions from a FLACS simulation of an 800-kg hydrogen explosion in a petrochemical plant. The ignition point is marked with a red circle in Figure 4a just to the right of the structure. The FLACS simulation assumed stoichiometric combustion at a 30% hydrogen concentration.

The pressure wave evolves radially away from the ignition point where the hydrogen was initially concentrated. Because of the structural obstruction, the pressure wave is asymmetric and stronger in the direction indicated by the arrow labeled B. As a result, pressure is greatest toward the B direction as is evident in Figure 4a. Even at some distance away, the effect of the structure and pipeline persists in the pressure distribution as shown in Figure 4d. Explosive overpressure is

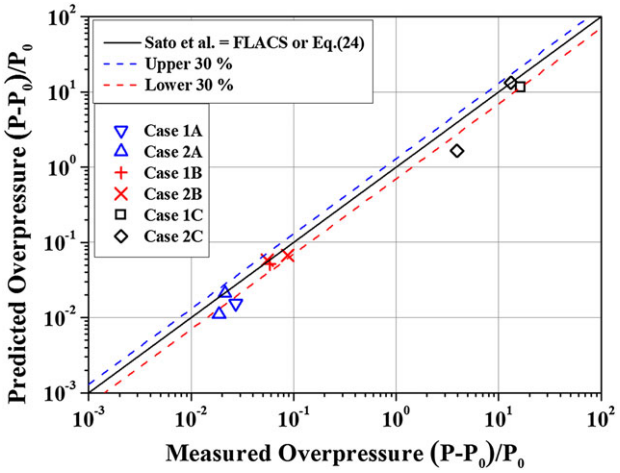

Figure 3. Cross plot of computational fluid dynamics and the analytical theory for overpressure estimates.

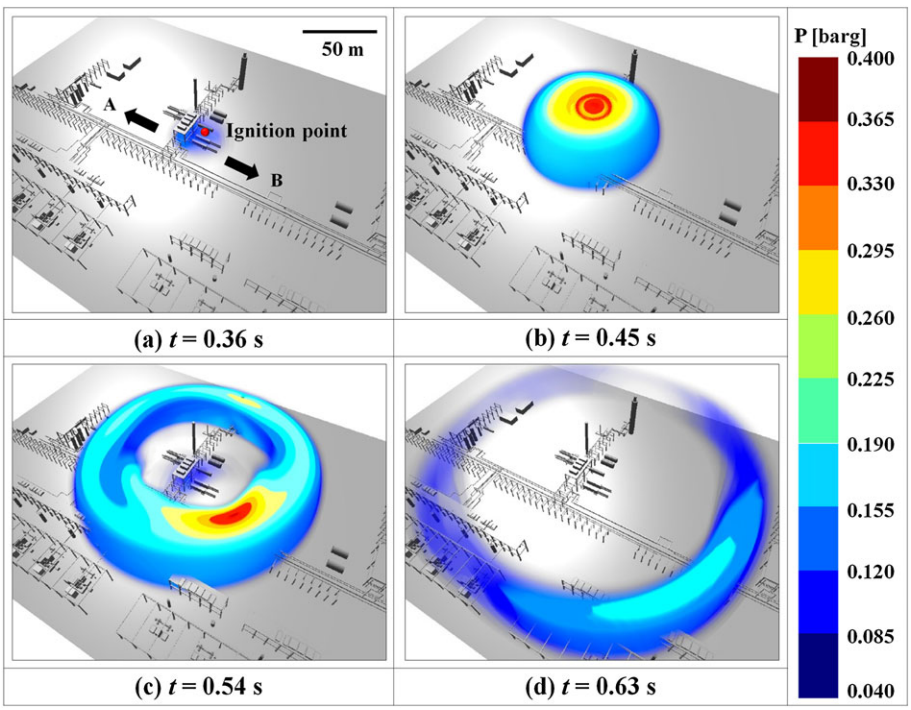

Figure 4. Pressure series for an 800-kg hydrogen explosion.

DOI: 10.1002/fam

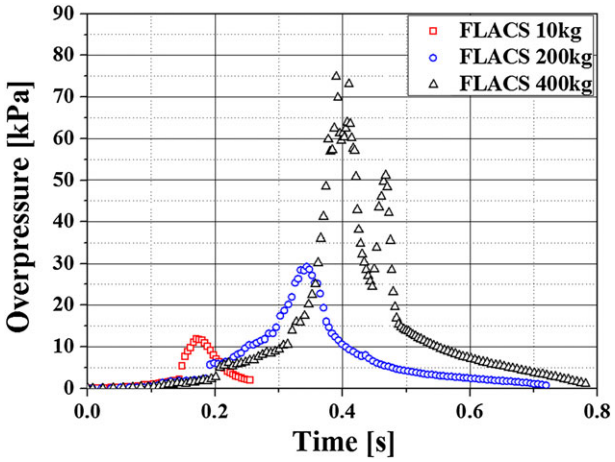

Figure 5. Maximum overpressures in the FLACS domain.

estimated both by FLACS (weak explosion or deflagration), which considers the effects of a real explosion scenario (it includes the effects of the 3D plant structures).

The amount of leaked hydrogen can vary depending upon different accident scenarios. For convenience, we have varied the hydrogen mass in the plausible range from 10 to 400 kg under open air condition. Figure 5 compares the highest overpressure values from a FLACS simulation for hydrogen explosions of $m = 10$, 200, and 400 kg. These overpressures are the maximum detected at a given time throughout the model domain. It is seen that a greater fuel mass yields a larger overpressure with a commensurately faster decrease in overpressure. The slope of the FLACS results seems to be relatively insensitive to the fuel mass change, at least, in the pressure reduction stage. The FLACS results more or less pertain to the similar pressure reduction rate. One noticeable difference in the FLACS simulation of the 400-kg explosion is the existence of a second overpressure peak. Because Figure 5 captures the maximum overpressure in the model domain, it is apparent that the plant structures can focus the overpressure into a local maximum. The corresponding data (black triangles in Figure 5) appear to be scattered over time in the 400-kg case. The scattered or 'dispersive' result is explained by the way the maximum pressure was recorded in the FLACS simulation. As mentioned previously, the local pressure can rise and fall by the local obstruction, in which flow stagnation and turbulence are generated. In FLACS simulation, the presence of the obstruction was implemented to emulate the real geometry of a petrochemical plant, yielding dramatic fluctuations at the pressure reduction stage, according to the sizes and locations of the obstructing objects. Therefore, the location of the maximum pressure is not fixed. It should be emphasized that FLACS simulation provides the reality of turbulence and presence of obstacles. The analytic solution can be cross-checked to assess the magnitude of the uncertainties associated with the FLACS solution. The cross-check is especially important as we seek to find the worst-case scenario for a conservative estimate (which can be obtained via the analytic solutions) for designing enduring and safe petrochemical plants.

4. CONCLUSIONS

Overpressure due to hydrogen explosions was estimated using the 3D computational code (FLACS) and the analytic solution based on the theory of strong explosion. These estimations were compared against the existing experimental data. The analytic solution was found to be appropriate to model the detonation case, where the chemical reaction behind the shock wave front rapidly fades and the later deteriorates to a pure shock wave, while FLACS was more appropriate to model the deflagration cases. The 3D numerical results accounted for the effect of the generated turbulent eddies on the flame propagation and the kinetics of the combustion reaction while the analytic solution did not consider these effects and concentrated on the shock wave propagation in the gas

DOI: 10.1002/fam

dynamical limit. This indicates that the turbulent eddies and the detailed kinetics effects were significant to affect the overall overpressure during deflagration. On the other hand, during detonation, the initial explosive energy of hydrogen released almost instantaneously was the most dominant factor that affected the overpressure. We found that the overpressure did not exceed the value of 1 bar for the hydrogen mass of <400 kg. The overpressure of less than 1 bar quickly dissipated and was equalized with the surrounding atmospheric pressure within a second; thus, the nearby surrounding structures will highly unlikely be damaged in this overpressure range.

ACKNOWLEDGEMENTS

This research was primarily supported by Daewoo Institute of Construction and Technology and partially supported by Technological Innovation R&D Program (S2314490) of SMBA Korea, and a special Korea University Grant. The author (S.S. Yoon) extends his appreciation to the Vice Deanship of Scientific Research at King Saud University.

REFERENCES

1. Coco J. *The 100 Largest Losses (1972–2001): Large Property Damage Losses in the Hydrocarbon-Chemical Industries. 20th Edition: Marsh Property Risk Consulting 20th Edition*. A Publication of Marsh's Risk Consulting Practice: New York 2003.
2. Kletz T. *What Went Wrong? Case Histories of Process Plant Disasters and How They Could Have Been Avoided*. Butterworth-Heinemann: Oxford, 2009.
3. Molkov VV, Makarov DV, Schneider H. Hydrogen–air deflagrations in open atmosphere: large eddy simulation analysis of experimental data. *International Journal of Hydrogen Energy* 2007; **32**(13):2198–2205.
4. Middha P, Hansen OR. Using computational fluid dynamics as a tool for hydrogen safety studies. *Journal of Loss Prevention in the Process Industries* 2009; **22**(3):295–302.
5. Davis SG, Engel D, Gavelli F, Hinze P, Hansen OR. Advanced methods for determining the origin of vapor cloud explosions case study: the 2006 Danvers anvers explosion investigation. *Fire Technology* 2014; **50**(4):823–850.
6. Garcia J, Baraldi D, Gallego E, Beccantini A, Crespo A, Hansen OR, Høiset S, Kotchourko A, Makarov D, Migoya E, Molkov V, Voort MM, Yanez J. An intercomparison exercise on the capabilities of CFD models to reproduce a large-scale hydrogen deflagration in open atmosphere. *International Journal of Hydrogen Energy* 2010; **35**(9):4435–4444.
7. Landau LD, Lifshitz EM. 1987. *Fluid Mechanics*. Volume **6** (Course of Theoretical Physics) Butterworth-Heinemann: Oxford.
8. Sedov LI. Propagation of strong blast waves. *Journal of Applied Mathematics and Mechanics* 1946; **10**:241–250.
9. Sedov LI. *Similarity and Dimensional Methods in Mechanics*. CRC Press: Boca Raton, 1993.
10. Taylor G. 1950. The formation of a blast wave by a very intense explosion. I. Theoretical discussion. *Proceedings of the Royal Society of London. Series A, Mathematical and Physical Sciences*, **201**(1065):159–174.
11. Taylor G. 1950. The formation of a blast wave by a very intense explosion. II. The atomic explosion of 1945. *Proceedings of the Royal Society of London. Series A, Mathematical and Physical Sciences*, **201**(1065):175–186.
12. von Neumann J. *The point source solution (Collected Works*, Vol. VI). Pergamon Press: Oxford 1963.
13. Yarin AL. *Self-similarity, Chapter 2.3 in Springer Handbook of Experimental Fluid Mechanics*. Springer: Heidelberg, 2007.
14. Sato Y, Iwabuchi H, Groethe M, Merilo E, Chiba S. Experiments on hydrogen deflagration. *Journal of Power Sources* 2006; **159**(1):144–148.
15. GexCon, *FLACS v10.2 User's Manual*. GexCon AS: Bergen, 2014.
16. Launder BE, Spalding DB. The numerical computation of turbulent flows. *Computer Methods in Applied Mechanics and Engineering* 1974; **3**(2):269–289.
17. Hjertager BH. Computer simulation of turbulent reactive gas dynamics. *Modeling, Identification and Control* 1984; **5**(4):211–236.
18. Hjertager BH. Three-dimensional modeling of flow, heat transfer and combustion. In *Handbook of Heat and Mass Transfer*. Gulf Publishing: Houston, 1986; 1303–1350.
19. Hjertager BH, Fuhre K, Bjørkhaug M. Gas explosion experiments in 1:33 and 1:5 scale offshore separator and compressor modules using stoichiometric homogeneous fuel/air clouds. *Journal of Loss Prevention in the Process Industries* 1988; **1**(4):197–205.
20. Patankar S. *Numerical Heat Transfer and Fluid Flow*. CRC Press: Boca Raton, 1980.
21. Zeldovich YB, Barenblatt GI, Librovich VB, Makhviladze GM. *The Mathematical Theory of Combustion and Explosions*. Consultants Bureau: New York, 1985.
22. Bray KNC. Studies of the turbulent burning velocity. *Proceedings of the Royal Society of London. Series A: Mathematical and Physical Sciences* 1990; **431**(1882):315–335.
23. Arntzen BJ. 1998. Modelling of turbulence and combustion for simulation of gas explosions in complex geometries. *Dr. Ing. Thesis*, NTNU, Trondheim.
24. Bang B, Park HS, Kim JH, Al-Deyab SS, Yarin AL, Yoon SS. Simplified method for estimating the effect of a hydrogen explosion on a nearby pipeline. *Journal of Loss Prevention in the Process Industries* 2016; **40**:112–116.
25. Sachs RG. 1944. The dependence of blast on ambient pressure and temperature: DTIC Document.

DOI: 10.1002/fam